J Solid State Electrochem (2007) 11:811–820
DOI 10.1007/s10008-006-0227-7

ORIGINAL PAPER

Simulation of oxygen evolution reaction at porous anode from flowing electrolytes

Mahmoud M. Saleh

Received: 25 August 2006 / Revised: 12 September 2006 / Accepted: 21 September 2006 / Published online: 9 January 2007

Abstract Oxygen evolution reaction (OER) at flow-through porous anode was simulated with the aid of a mathematical model. The OER was assumed to be the only reaction that takes place at the electrode. The model accounts for effects of the kinetics, ohmic, hydrodynamics, and structural parameters and bubble formation on the potential and current distributions within the electrode and on the overall performance of the electrode. The latter was evaluated via interpretation of the polarization curves of the OER at the porous anode. The model results were discussed in the light of some controlling dimensionless groups. The conductivities of both the electrolyte and the solid matrix have dramatic effects on the general behavior of the porous anode, and lower performance of the electrode was observed when both and/or one of them have limited conductivity values. The electrode potential, and hence the power required to attain a specific current (rate), is highly dependent on the degree of bubble formation within the bed matrix. The model predictions were compared with collected experimental data of OER from flowing sulfuric acid solution at Pt-loaded reticulated vitreous carbon. Good agreements were obtained at the employed experimental conditions. The present work helped to understand the anode performance for further application for simultaneous gas evolution, e.g., O_2 and O_3 gases.

Keywords Oxygen · Anode · Mathematical modeling · Bubbles · Porous

M. M. Saleh (✉)
Chemistry Department, Faculty of Science, Cairo University, Cairo, Egypt
e-mail: mahmoudsaleh90@yahoo.com

Introduction

Mathematical modeling of three-phase (gas–liquid–solid), three-dimension porous electrodes has always been an important way to understand the behavior of such systems [1, 2]. Porous electrode is the heart of many technological and industrial applications such as fuel cells, water treatment, and electrolysis cells [3–5]. While measurements on such systems and optimization could face physical limitations, mathematical modeling of such systems can introduce insight and guidelines for the optimization and design of such systems [6, 7]. Oxygen evolution reaction (OER) represents a core process in the field of electrochemistry. Not only does OER represent an academic interest, but also technological processes such as chlor-alkali [8] and ozone production [9] represent processes that rely on understanding the OER. While proper anodes for selective generation of pure oxygen [10] was reported, dimensionally stable anodes (DSA) were introduced to increase the OER polarization in favor of Cl_2 [11] or O_3 [12] gas. Although OER has been studied extensively at planar electrodes [13–15], the studies at porous electrodes are limited [16]. Although some authors studied the OER at rough [17] or porous electrodes [18], no author has studied (to the best of our knowledge) OER from flowing solution at porous electrodes. Flow-through porous electrodes offer high values of surface-to-volume ratio and, hence, reduce the space required to attain a specific rate. Porous electrodes are typically made with conductive materials, but these may degrade under high temperatures or anodic potential conditions. This problem is of less importance for fuel-cell anode catalysts, which operate at relatively low potentials, but it can be quite significant for electrolyzers [19]. In previous modeling of gas evolving flow-through porous cathode, the effect of the matrix phase conductivity was

considered to be negligible with respect to the electrolyte phase conductivity [20, 21]. In other applications such as anodic oxygen, ozone, or chlorine generation, there is a growing trend to use so-called dimensionally stable anodes (DSA), which contain oxides in its structures; hence, its conductivity may not be considered as negligible [22, 23].

It is the aim of the present work to simulate the OER reaction at flow-through porous anode. The model is developed to account for different effects of kinetics, ohmic, hydrodynamics, and structural parameters and gas bubble formation on the general electrode performance and on the current and potential distributions within the electrode bed. The model validity is tested by comparing its predictions with collected polarization curves of OER from flowing sulfuric acid solution at Pt-loaded reticulated vitreous carbon. This study is a first step in the application of such systems for simultaneous evolution of O_2/Cl_2 or O_2/O_3 systems.

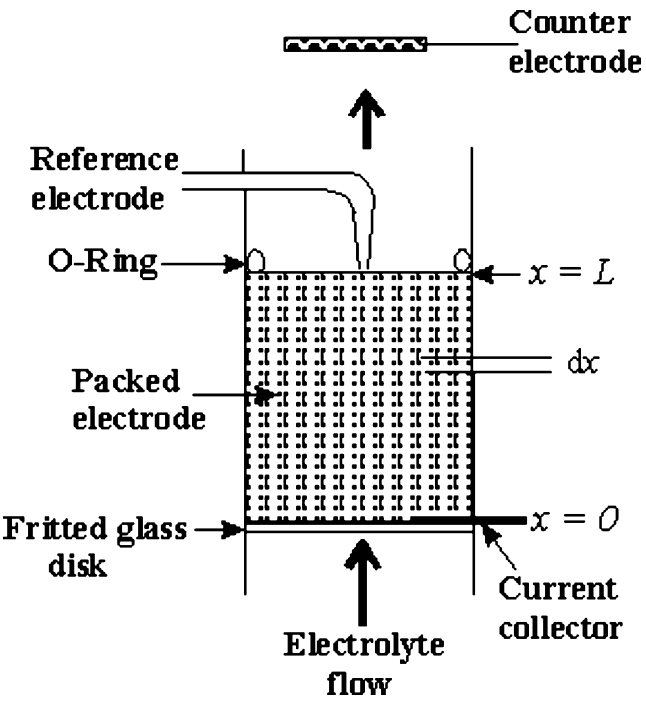

Fig. 1 Schematic of the cell arrangement and flow direction

Mathematical model

The electrochemical oxygen evolution reaction at the porous anode can be represented as;

$$2H_2O = O_2 + 4H^+ + 4e \quad U^0 = 1.23\,V \tag{1}$$

The mathematical model was developed under the following conditions. The porous electrode is considered to consist of a continuum of two phases: each phase is either pure ionic or electronic conductor [24]. The reaction is of zero order with respect to the reactant and involves an electron rate-determining step and is only charge-transfer controlled. It is assumed that the porous matrix has a uniform porosity, θ, and does not undergo anodic dissolution. The model is one-dimensional; hence, the variables are functions only of the x direction. Figure 1 shows the porous electrode arrangement and direction of flow.

The mechanism for OER can be represented by the following elementary steps [25, 26]:

$$H_2O = (OH^{\bullet})_{ads} + H^+ + e^- \text{ rate determining step} \tag{2}$$

$$(OH^{\bullet})_{ads} = (O^{\bullet})_{ads} + H^+ + e^- \tag{3}$$

$$2(O^{\bullet})_{ads} = O_2 \tag{4}$$

Taking step 2 as the rate-determining step, one can write the Butler–Volmer expression as [26, 27]:

$$\frac{di_2(x)}{dx} = i_o a\left[(1-\omega_{OH^{\bullet}})[H_2O]e^{\alpha(\Phi_1-\Phi_2-U_{rev})/b} - \omega_{OH^{\bullet}}e^{-(1-\alpha)(\Phi_1-\Phi_2-U_{rev})/b}\right] \tag{5}$$

Considering $OH^{\bullet}$ – surface concentration ($\omega_{OH^{\bullet}} \to 0$) [26] as negligible, for conditions of the high-field approximation [for $(\Phi_1-\Phi_2-U_{rev})\geq 0.1$ V], Eq. 5 is reduced to:

$$\frac{di_2(x)}{dx} = i_o\, a\left[e^{\alpha(\Phi_1-\Phi_2-U_{rev})}\right] \tag{6}$$

where di_2/dx is the gradient of the ionic current that enters the pore solution, Φ_1 and Φ_2 are the potentials of the solid phase and the solution phase, respectively, and U_{rev} is the reversible electrode potential. Ohm's law governs the ionic current in the solution phase, i_2, with the gradient of the potential in the solution phase by:

$$i_2(x) = -\kappa(x)\frac{d\Phi_2}{dx} \tag{7}$$

where $\kappa(x)$ is the pore electrolyte conductivity that varies with the distance inside the bed. It depends on the composition and extent of bubble generation within the pore electrolyte (see Eq. 11). The gradient of potential inside the solid phase is related to the electronic current, $(i_1(x)$ by:

$$i_1(x) = -\sigma_{eff}\frac{d\Phi_1}{dx} \tag{8}$$

where σ_{eff} is the effective conductivity of the porous bed that is given by [28]:

$$\sigma_{eff} = \sigma[1-\theta]^{1.5} \tag{9}$$

where σ is the conductivity of the solid matrix. A mathematical expression of the sum of the divergences of

the solution and matrix current densities as a consequence of the electroneutrality is given by [24]

$$\frac{di_1(x)}{dx} + \frac{di_2(x)}{dx} = 0 \tag{10}$$

Bruggeman's equation can be used to correlate the pore electrolyte conductivity, $\kappa(x)$ with the electrolyte conductivity in the bulk outside the pores, κ^o, by [21, 29]:

$$\kappa(x) = \kappa^o[\theta - \varepsilon(x)]^{1.5} \tag{11}$$

where $\varepsilon(x)$ is the gas void fraction that is related to the solution current by:

$$\varepsilon(x) = \frac{\theta i_2(x)}{\upsilon\lambda + i_2(x)} \tag{12}$$

where υ is the superficial flow rate and λ is the coefficient of faradaic gas generation, which is a factor converting the solution current to volume of the generating gas bubbles, such that [21]:

$$\lambda = \frac{4PF}{RT} \tag{13}$$

Assuming four faradaic electrons per 1 mol of the evolved gas (as the number 4 appears in Eq. 13) and assuming ideal gas behavior, λ equals 15.8 C cm^{-3} at standard temperature and pressure.

Equations 6–8, 10–12 describe the behavior of the system and give the distributions of the variables i_1, i_2, Φ_1, Φ_2, κ, and ε within the porous electrode. Substituting the dimensionless variables $\bar{i} = i/I_o$, $\overline{\Phi} = \Phi/b$, $\overline{\kappa} = \frac{\kappa}{\kappa^o}$ and $y = x/L$, one can obtain the system of equations in dimensionless form as follows:

$$\frac{d\bar{i}_2(y)}{dy} = e^{\alpha(\overline{\Phi}_1 - \overline{\Phi}_2 - \overline{U}_{rev})} \tag{14}$$

$$\bar{i}_2(y) = -S_k\overline{\kappa}(y)\frac{d\overline{\Phi}_2}{dy} \tag{15}$$

$$\bar{i}_1(y) = -S_\sigma\frac{d\overline{\Phi}_1}{dy} \tag{16}$$

$$\frac{d\bar{i}_1}{dy} + \frac{d\bar{i}_2}{dy} = 0 \tag{17}$$

Table 1 Definitions of the controlling groups and parameters

Group	Definition
$S_\kappa = \kappa^o b/I_o L$	Dimensionless solution conductivity group
$S\sigma = \sigma_{eff} b/I_o L$	Dimensionless matrix conductivity group
$I_o = i_o aL$	Total exchange current density
$\Psi = \upsilon\lambda/I_o$	Dimensionless bubble group
α=0.5[a]	Charge transfer coefficient
θ=0.7	Porosity
$\overline{U}_{rev} = 1.23/b$[a]	Dimensionless reversible electrode potential.

[a] This value was used only for theoretical calculations.

Table 2 Values of the parameters used in fitting the experimental data in Fig. 8

Parameters	
a=40 cm^2 cm^{-3}	i_o=1×10^{-9} A cm^{-2}
L=3.0 cm	α=0.3
θ=0.90	T=298 K
υ=0.09 cm s^{-1}	σ=5×10^3 ohm^{-1} cm^{-1}
[H_2SO_4]/M	κ^o/Ω^{-1} cm^{-1}[37]
0.1	0.05
0.5	0.25
2.0	0.78

$$\overline{\kappa}(y) = [\theta - \varepsilon(y)]^{1.5} \tag{18}$$

$$\varepsilon(y) = \frac{\theta\bar{i}_2(x)}{\Psi + \bar{i}_2(x)} \tag{19}$$

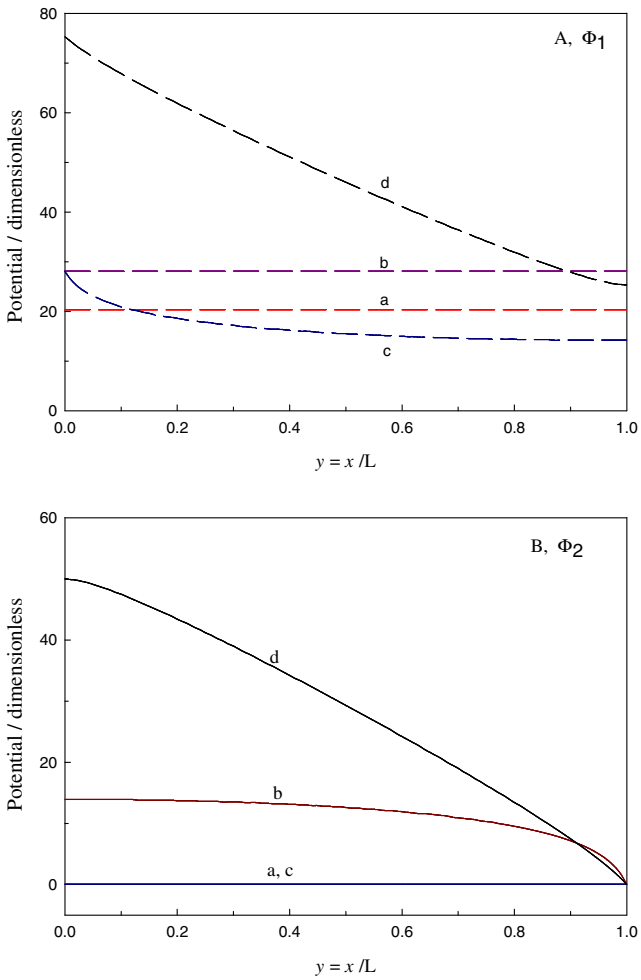

Fig. 2 Distributions of the dimensionless potential of the solid matrix, Φ_1 (**A**) and the dimensionless potential of solution, Φ_2 (**B**) at different values of S_κ and S_σ at dimensionless cell current=0.5/I_o and I_o=2×10^{-5}. *a* S_κ, S_σ = 2.5×10^6, 2.5×10^6, *b* 1.25×10^2, 2.5×10^6, *c* 2.5×10^6, 1.25×10^2 and *d* 2.5×10^2, 2.5×10^2. Bubble formation is not included

Equations 14–19 represent the model equation system in a dimensionless form and lead to some dimensional and dimensionless groups and parameters (listed in Table 1). The boundary conditions for the above system are:

1. at $y=0$ (see reference [30])

$$\bar{i}_2 = 0,\ \frac{d\,\overline{\Phi}_1}{d\,y} = -\frac{i_{\text{cell}}}{I_o.S_\sigma},\ \varepsilon = 0 \text{ and } \kappa = \theta^{1.5} \tag{20}$$

2. at $y=1$

$$\bar{i}_1 = 0,\ \overline{\Phi}_2 = 0 \tag{21}$$

Equations 14–19, along with the boundary conditions 20 and 21, were solved with a numerical technique developed by Newman [31]. For simplicity, the bars over the dimensionless variables are going to be dropped in the coming discussion.

Materials and methods

Reticulated vitreous carbon (RVC) blocks of grade 60 pore per linear inch (PPI) were supplied by Electrosynthesis (New York) and were used as received. Porous RVC block was cut in a cylinder using a hollow cylindrical brass, cork-boring tool. This gave the required dimensions to fit the electrode chamber. The specifications of the RVC electrode are given in Table 2. It is held down tightly with a rubber O-ring onto the fritted glass disc to ensure good contact to the current collector and to eliminate the possibility of floatation. Figure 1 shows the cell and experimental arrangements of the flow-through porous electrode. The upper part of the cell presses the rubber O-ring. The electrolytic cell was essentially a cylindrical glass tube, which is held upright. The electrolyte was forced from the bottom (entry face) of the cell using a variable speed pump. The working electrode was polarized using a platinum screen as a counter electrode placed downstream with respect to the electrolyte flow. The potential at the exit face of the electrode, U (facing the counter electrode), was measured against the reference electrode [Ag/AgCl (NaCl sat.)]. An EG&G potentiostat/galvanostat model 273A controlled by m352 electrochemical software was used in all measurements.

The RVC electrode was of cylindrical dimensions of specific surface area, S, of 40 cm^{-1}, diameter of 1.5 cm, and a thickness, L, of 3 cm. It was electroplated with platinum from flowing recirculated 0.1 M H_2SO_4 solution containing 20 mM hexachloroplatinate. The same flow cell mentioned above was used in the in situ platinum electroplating process. Specific conditions such as low flow rate (0.04 cm s^{-1}) and low potential (0.0 V vs Ag/AgCl) were applied for 1 h to obtain the possible uniform Pt deposition within the bed [32, 33]. Assuming 100% current efficiency and using Faraday's law, the amount of deposited platinum was estimated from the amount of charge passed (70.0 C) to be 6.5 mg cm^{-3} of the RVC matrix. The current density presented in this study was taken on the basis of the geometric cross-sectional area of the RVC electrode (i.e., 1.80 cm^2). The SEM micrographs were taken on a JEOL JSM-20 scanning electron microscope.

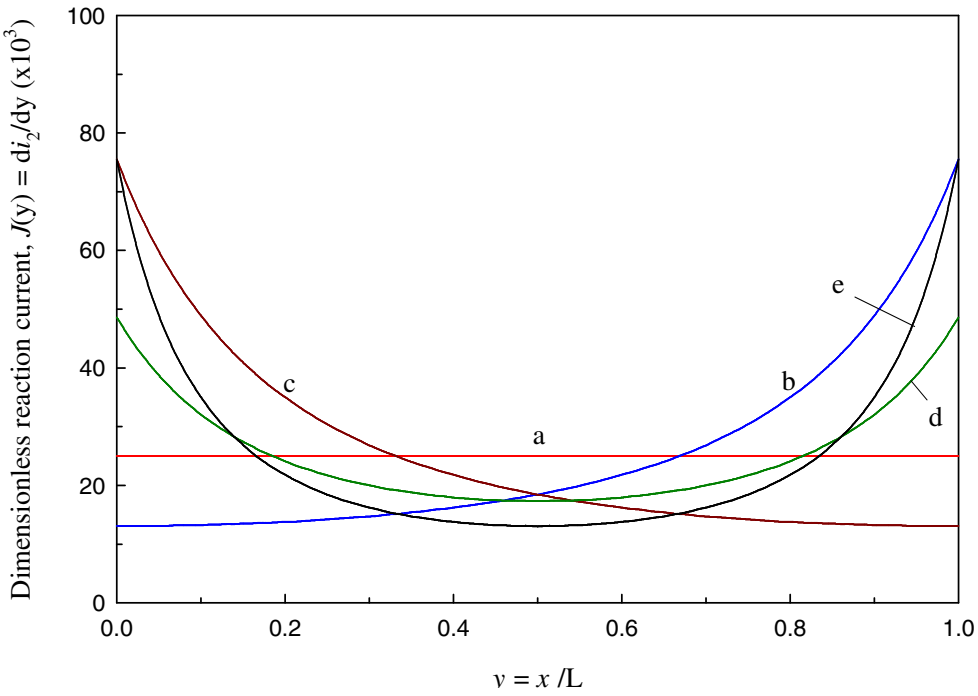

Fig. 3 Distributions of the dimensionless reaction current, $J(y)$ at different values of S_κ and S_σ at dimensionless cell current = $0.5/I_o$ and $I_o=2\times10^{-5}$. *a* S_κ, S_σ = 2.5×10^6, 2.5×10^6, *b* 1.25×10^2, 2.5×10^6, *c* 2.5×10^6, 1.25×10^2, *d* 2.5×10^2, 2.5×10^2, *e* 1.25×10^2, 1.25×10^2. Bubble formation is not included

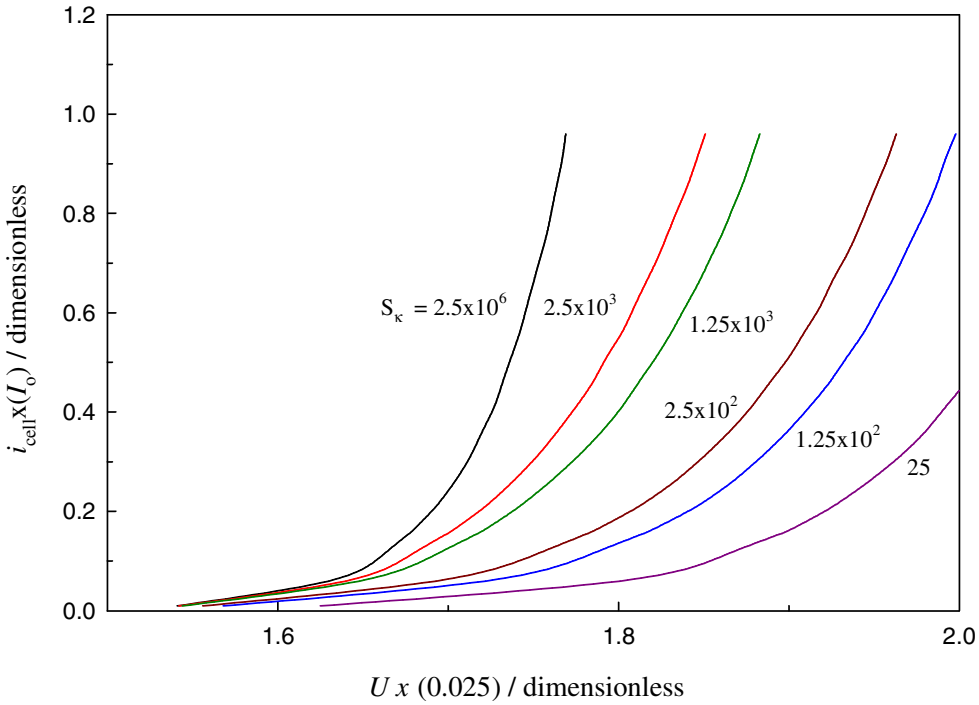

Fig. 4 Polarization curves of the OER at a fixed value of $S_\sigma=2.5\times10^6$ at different values of S_k using $I_o=2\times10^{-5}$. Bubble formation is not included

Results and discussion

Theoretical results

The theoretical results are presented in order to study the effects of the different controlling groups on the current and potential distributions within the porous electrode and also on the general performance of the electrode. The latter was evaluated via plots of the polarization curves of OER. Since the kinetics of the reaction were discussed elsewhere [34], we are going to concentrate here on the effects of the relative values of the conductivity groups of the solution S_κ and the matrix S_σ at different impacts of bubble formation.

Figure 2 shows the effects of the different values of S_κ and S_σ on the distributions of the matrix potential Φ_1 and the solution potential Φ_2, when the dimensionless cell

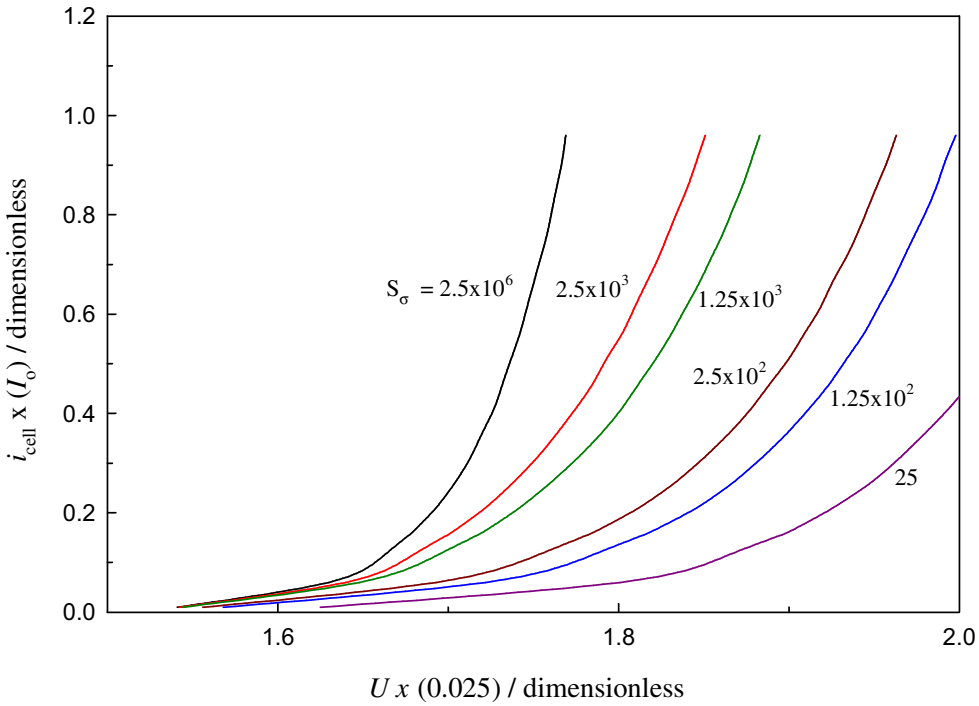

Fig. 5 Polarization curves of the OER at a fixed value of $S_k=2.5\times10^6$ at different values of S_σ using $I_o=2\times10^{-5}$. Bubble formation is not included

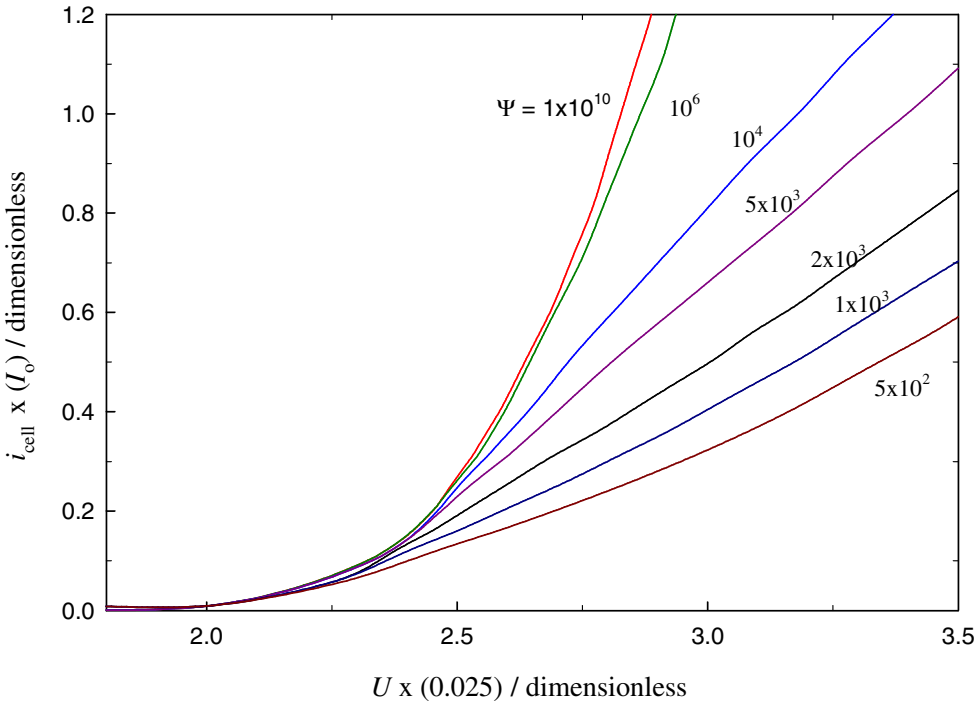

Fig. 6 Polarization curves of the OER at different values of the bubble group, Ψ using S_k and S_σ equals 50, 5, respectively and $I_o=2\times10^{-5}$

current=$0.5/I_o$. The plots of Figs. 2, 3, 4, 5, were constructed with the condition that the bubble formation is not included in the simulation. This was done by setting the bubble group Ψ as an infinite value in Eq. 19. Higher values of S_κ and S_σ mean higher values of κ^o and σ_{eff}, respectively and/or smaller I_o and L (see Table 1). As the value of S_κ and S_σ approached infinite value (case a), the potential Φ_1 and Φ_2, respectively, are uniformly distributed within the electrode bed. Different distribution profiles of both potentials were obtained as a consequence of the different combinations of limited values of S_κ and S_σ. Consider case b where S_κ is limited (1.25×10^2) and S_σ is not (1.25×10^6). At the back of the electrode (y=0), the current is carried mainly by the solid matrix and since S_σ is infinite and according to Eq. 16 the potential Φ_1 is uniform within the whole bed. Since S_κ is limited, at the back of the electrode low current is carried by the solution resulting in uniform Φ_2 at the back. On going towards the front of the electrode, the solution current increases and most of the current is carried by the solution leading to a nonuniform distribution of the solution potential Φ_2. The other cases can be discussed similarly.

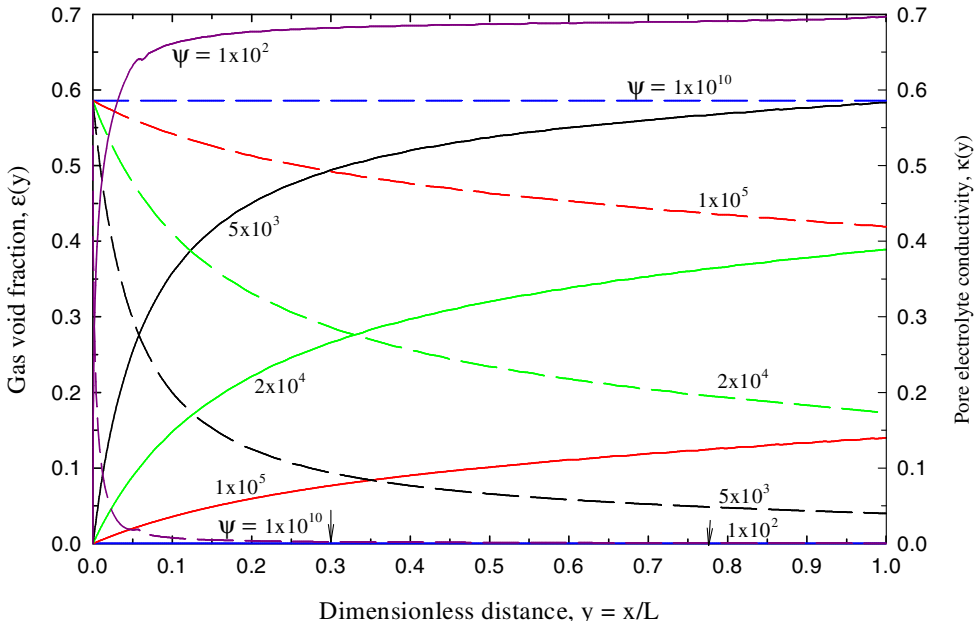

Fig. 7 Distributions of the gas void fraction, $\varepsilon(y)$ and the dimensionless pore electrolyte conductivity $\kappa(y)$ at a different bubble group, χ and at dimensionless cell current=$0.5/I_o$ and $I_o=2\times10^{-5}$. S_k and S_σ equals 50, 5, respectively. *Solidlines* are $\varepsilon(y)$ and *dashed lines* are $\kappa(y)$

The gradient of the solution current di_2/dx is the reaction current per unit volume, $J(x)$ and in dimensionless form equals $J(y)=di_2/dy$. The effect of the above combinations of S_K and S_σ on the reaction current distributions $J(y)$ is shown in Fig. 3. When S_K and S_σ are infinite (a rather hypothetical case), the reaction is completely uniform and full utilization of the bed is obtained. When S_K is limited, the reaction is pushed towards the front of the electrode (at $y=1$), and when S_σ is limited, the reaction is pushed towards the back of the electrode ($y=0$). Note that the driving force of the reaction is controlled by the difference in potential ($\Phi_1-\Phi_2$); hence, the potential distributions in Fig. 2 can interpret the present distributions of the reaction current in Fig. 3. Pushing the reaction towards one end of the porous anode in a gas-generating electrode has different effects than at other electrode systems. For instance, pushing the current in a porous cathode operating for metal deposition is affecting by plugging the porous electrode by metal deposits that preferentially and locally occur at one side. This can resist the electrolyte flow. For gas-evolving electrode, pushing the current to the back of the electrode may result in traveling of the bubbles within the whole bed. In both cases, lower utilization of the available electrode surface area is obtained. The minimum in $J(y)$ in Fig. 3 at a limited value of both S_K and S_σ is a result of the nonuniform distributions of Φ_1 and Φ_2, as in case d in Fig. 2. The minimum has been observed in the literature [35].

To study the effects of the above combinations of S_K and S_σ on the overall performance of the electrode, polarization curves were simulated for oxygen reaction at the above different combinations of S_K and S_σ similar to the above. Figures 4 and 5 show the effects of S_K and S_σ on the polarization curves of OER (bubble formation is not included). From porous electrode literature, the model results may be presented at constant current condition (galvanostatic) and obtain (measure) the electrode potential or at constant potential (potentiostatic) condition and obtain the cell current. In our case, a constant current was used and the electrode potential was obtained. The electrode potential U is taken as $\Phi_1|_{y=0}$ [30, 36]. The plots were constructed using the same parameters used in Figs. 2, 3. Figure 4 shows the effects of S_K at constant S_σ. As S_K increases, the potential required to attain a specific reaction current (rate) decreases. Figure 5 shows the effects of S_σ at constant value of S_K. From Figs. 4 and 5, the following conclusions can be derived. As S_K and/or S_σ increases, the potential required to sustain specific current (rate) decreases. The above decrease in the potential exerts an influence on the power required to obtain specific rates of the oxygen evolution reaction. The effects of the increase in S_K are equivalent to the increase in S_σ. While it is possible to increase the value of S_K by increasing the solution conductivity, it is not possible to increase the conductivity of the solid matrix conductivity. This is quite true as we use dimensionally stable anodes that have some oxide in its structure; hence, low conductivity is most likely to prevail.

The above results (Figs. 2, 3, 4, and 5) were simulated with no account of gas bubbles. Since we study a gas-evolving electrode, we should account for gas bubble formation within the pore electrolyte. The gas bubble formation reduces the cross-sectional area available for ionic flow and consequently decreases the effective conductivity of the pore electrolyte (see Eqs. 11 and 18). The gas bubble formation can be included in the model

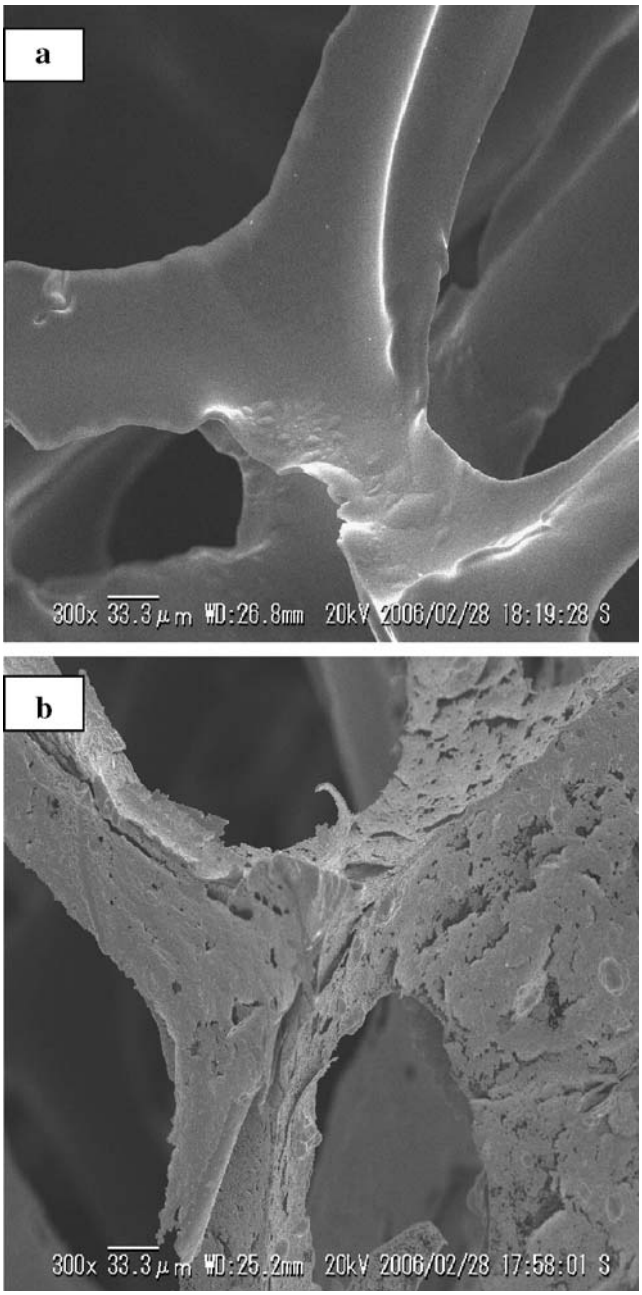

Fig. 8 SEM images of plain RVC (**a**) and RVC/Pt (**b**)

simulation by inserting finite values of the bubble group Ψ in the system equations.

Figure 6 shows polarization curves of the OER at different values of Ψ at S_κ and S_σ equal to 50 and 5, respectively. These values were chosen to simulate a closer case to the real situation, where DSA of lower matrix conductivity can be used for OER. As Ψ increases, the potential required to sustain specific current (rate) of the OER decreases. Note that there is a negligible difference between the polarization curve at $\Psi=10^{10}$ and at $\Psi=10^{5}$, pointing to the negligible degree of bubble formation. Higher values of Ψ mean higher values of the flow rate υ, and/or lower values of the total exchange current density I_o. While the former (υ) depends on the hydrodynamics of the system, the latter depends in the kinetics (i_o) and structural parameters (a and L; see Table 1). At lower values of Ψ, significant amounts of the gas bubbles accumulate inside the porous electrode leading to a decrease in the pore electrolyte conductivity. This is illustrated in Fig. 7. The figure shows the distributions of the gas void fraction, $\varepsilon(y)$, and the pore electrolyte conductivity, $\kappa(y)$, at S_κ and S_σ equal to 50 and 5, respectively, for which the same parameters used in Fig. 6. Note that since S_σ is relatively limited with respect to S_κ, the reaction is pushed towards the back of the electrode (compare Fig. 3, case c). This causes the formed bubbles to travel along the electrode from the back ($y=0$) to the front of the electrode. At constant kinetic and structural parameters, the flow rate is an important operating parameter. At higher flow rates (higher Ψ) lower potentials are obtained; hence, a lower power requirement can be achieved to obtain the specific rate of the process. Higher flow rates help to sweep the bubbles out of the electrode bed leading to lower polarization. However, higher flow rates may cause lower concentrations of a desirable gas product in the outlet streams. The last point is crucial when dealing with simultaneous generation of a desirable gas, e.g., ozone or chlorine. This calls for further mathematical modeling to optimize the system to avoid higher polarization and, at the same time, obtain considerable concentrations of desirable flowing aqueous gas solutions.

Testing for the validity of the model

The model was tested by comparing the theoretical results with the experimental data for oxygen evolution reaction at RVC/Pt from flowing H_2SO_4 solutions of different concentrations (0.1–2 M). The dimensional model (Eqs. 6–8, 10–12) was solved using the fitting parameters shown in Table 2. SEM images of RVC and RVC/Pt are shown in Fig. 8a and b, respectively. Platinum loadings are quite obvious on the RVC matrix. Since the conductivity of the sulfuric acid solution increases with concentration at the studied range [37], it is feasible to test the effects of the solution conductivity at fixed matrix conductivity. Polarization curves for OER are shown in Fig. 9. The symbols are experimental data and the solid and dashed lines are the model predictions including and

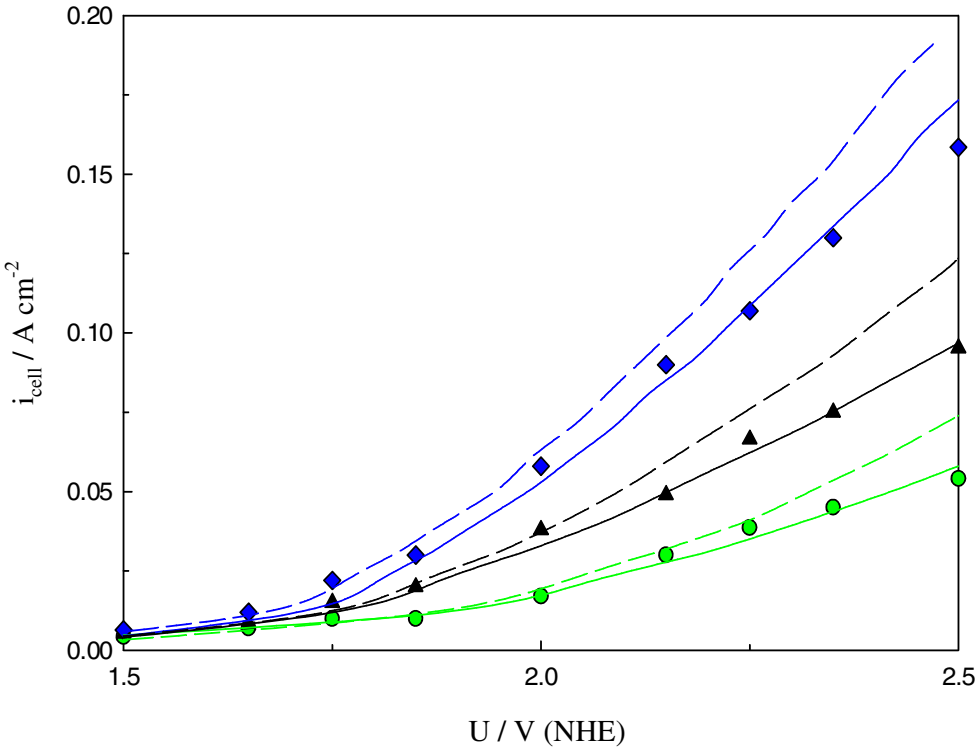

Fig. 9 Polarization curves of OER at RVC/Pt anode at different H_2SO_4 concentrations and υ of 0.09 cm s^{-1}. *Symbols* are the experimental data and *solid lines* and *dashed lines* are model calculations with and without including the bubble effects in the model. Symbols are for 0.1 M (*shaded circle*), 0.5 M (*shaded triangle*) and 2 M H_2SO_4 (*shaded square*)

not including the bubble formation, respectively. Table 2 shows the fitting parameters, which were used in fitting the model calculations with the experimental polarization curves. Equation 9 was used to estimate the effective solid conductivity of the solid matrix. The reversible electrode potential U_{rev} was calculated using the equation;

$$U_{rev} = 1.23 - 0.0591\,\mathrm{pH} \quad (22)$$

The values of U_{rev} at different acid concentration are close to 1.20 V.

The values of a, θ, and σ, shown in Table 2, were used as received by the company. The parameters L, T, and υ are operating and structural parameters. The value of α and then the value of i_o were used in fitting the data of the polarization curve at 0.1 M H_2SO_4 and then they were used without further modification in the other curves, i.e., at 0.5 and 2 M H_2SO_4. The value of κ^o was changed with the acid concentration as shown in Table 2. The i_o value of OER is about an order of magnitude less than the reported value of pure Pt at similar conditions [38]. This can be attributed to the fact that a full coverage of RVC with Pt is not guaranteed at the present conditions and yet some carbon surface participates in the OER. As the concentration (conductivity) of the H_2SO_4 solution increases the potential required to obtain specific current (rate) decreases. The model predictions show good agreement with the experimental data. It is noteworthy to mention that the bubble effects should be taken into consideration for the gas generating electrodes, otherwise erroneous results can be obtained. When the bubble effects are not included in the model calculations (as shown in the dashed lines in Fig. 9) higher currents were obtained than when they are included in the model calculations (solid lines).

Summary and conclusions

Oxygen evolution reaction was simulated at flow-through porous anode. The model predictions showed the impacts of different combinations of the solution and matrix conductivity in the absence and presence of gas bubble formation. The potential required to attain a certain current (rate) of the oxygen evolution decreases as both and/or one of the conductivity group increases and/or the bubble group increases. The model predictions were compared with experimental data of OER at RVC/Pt anode in flowing sulfuric acid solutions. A set of parameters was used in the fitting procedure. Good agreement was obtained and erroneous results are obtained if the bubble effects were not included in the simulations. The present results call for future mathematical modeling and experiments to optimize concentrations of a desired gaseous product with the possible lower potentials.

a	Specific surface area, $cm^2\ cm^{-3}$
b	RT/F, V
F	Faraday's constant, 96,500 C mol^{-1}
i_{cell}	Applied cell current per unit cross-sectional area of the packed bed, A cm^{-2}
i_1	Superficial local matrix current density (based on cross section circular geometric area), A cm^{-2}
i_2	Superficial local solution (ionic) current density (based on cross section circular geometric area), A cm^{-2}
I_o	Total exchange current density, $i_o aL$
i_o	Exchange current density based on the reaction area, A cm^{-2}
J	Local reaction current per unit volume of the packed bed, A cm^{-3}
S_κ	Dimensionless solution conductivity group
S_σ	Dimensionless matrix conductivity group
L	Electrode thickness, cm
P	Pressure, atm
U_{rev}	Reversible electrode potential, V
U	Electrode potential, V
υ	Electrolyte flow velocity, cm s^{-1}
R	Gas constant, 82.06 (cm^3 atm)/(mol K^{-1})
T	Absolute temperature, K
y	Dimensionless distance within the electrode, x/L
α	Charge transfer coefficient of the electrochemical reaction
λ	Constant, $4PF/RT$, C cm^{-3}
ε	Gas void fraction of the pore volume, dimensionless, Eq. 8
κ^o	Electrolyte conductivity in the bulk outside the pores, $\Omega^{-1}\ cm^{-1}$.
σ	Matrix conductivity, $\Omega^{-1}\ cm^{-1}$
σ_{eff}	Effective matrix conductivity, $\Omega^{-1}\ cm^{-1}$
$\kappa(x)$	Pore electrolyte conductivity, $\Omega^{-1}\ cm^{-1}$.
Φ_1	Potential in the matrix phase, V
Φ_2	Potential in the solution, V
Ψ	Dimensionless bubble group
θ	Porosity
$\omega_{OH^\bullet}$	Fraction of surface covered with adsorbed $OH^\bullet$

References

1. Devan S, Subramanian VR, White RE (2004) J Electrochem Soc 151:A905
2. Du CY, Cheng XQ, Yang T, Yin GP, Shi PF (2005) Electrochem Commun 7:1411
3. Pilone D, Kelsall GH (2006) J Electrochem Soc 153:D85
4. Friedrich JM, Ponce-de-Leon CG, Reads W, Walsh FC (2004) J Electroanal Chem 151:203

5. Yu H, Scott K (2004) Electrochem Commun 6:361
6. Saleh MM (1999) Electrochim Acta 45:959
7. Dukovic J, Tobias CW (1987) J Electrochem Soc 134:331
8. Gorodetskii VV, Russ (2003) J Electrochem Soc 39:650
9. Kraft A, Stadelmann M, Wunsche M, Blaschke M (2006) Electrochem Commun 8:883
10. Fujimura K, Izumiy K, Kawashima A, Akiuama E, Habazaki E, Kumagai N (1999) J Appl Electrochem 29:765
11. Pilalla AS, Cobo EO, Duarte ME, Salinas DR (1997) J Appl Electrochem 27:1283
12. Santana MHP, Silva LMD, De Faria LA, Boodts JFC (2003) Electrochim Acta 49:1935
13. Comninellis C, Vercesi GP (1991) J Appl Electrochem 21:335
14. Tatapudi P, Fenton JM (1994) J Electrochem Soc 141:1174
15. Wang YH, Cheng S, Chan K, Li XY (2005) J Electrochem Soc 152:D197
16. Saleh MM, Awad MI, Ohsaka T (2006) Electrochim Acta 51:6331
17. Huet F, Musiani M, Nogueira RP (2004) J Solid State Electrochem 8:786
18. Heidrich H, Muller L, Polovchenko BI (1990) J Appl Electrochem 20:686
19. Waraksa CC, Chen G, Macdonald DD (2003) J Electrochem Soc 150:E429
20. Ateya GB, El-Anadouli B (1991) J Electrochem Soc 138:1331
21. Saleh MM, Weidner JW, Ateya BG (1995) J Electrochem Soc 142:4113
22. Silva LMD, Franco DV, Forti JC, Jardim WF, Boodts JFC (2006) J Appl Electrochem 36:523
23. Katsuki N, Takahashi E, Toyoda M, Kurosu T, Lida M, J Electrochem Soc 145:2358
24. Duan T, Weidner JW, White RE (2002) J Power Sources 107:24
25. Pavlov P, Monahov B (1996) J Electrochem Soc 143:3616
26. Silva LMD, De Faria LA, Boodts JFC (2003) Electrochim Acta 48:699
27. Bard AJ, Faulkner LR (1980) Electrochemical methods. Wiley, New York, p 96
28. Devan S, Subramanian VR, White RE (2004) J Electrochem Soc 151:A905
29. Meredith RE, Tobias CW (1962) In: Gerischer H, Tobias CW (eds) Conduction in heterogeneous systems. Advances in electrochemistry and electrochemical engineering, vol 2. Wiley, New York, pp 17–48
30. Doherty T, Sunderland JG, Roberts EPL, Pickett DJ (1996) Electrochim Acta 41:519
31. Newman J (1991) Electrochemical systems, 2nd edn. Prentice-Hall, Englewood Cliffs, NJ, p 552
32. Alkire R, Gracon B (1975) J Electrochem Soc 122:1594
33. Trainham JA, Newman J (1977) J Electrochem Soc 124:1528
34. Saleh MM (2004) J Phys Chem B 108:13419
35. Trainham JA, Newman J (1978) J Electrochem Soc 125:58
36. Cheng CY, Kelsall GH, Pilone D (2005) J Appl Electrochem 35:1191
37. Dobos D (1975) Electrochemical data. Elsevier, New York, p 512
38. Jiang J, Yi B (2005) J Electroanal Chem 577:107